Engineering 23 (2023) 82–89

Contents lists available at ScienceDirect

Engineering

journal homepage: www.elsevier.com/locate/eng

Research
Material Science and Engineering—Article

AIE-Active Freeze-Tolerant Hydrogels Enable Multistage Information Encryption and Decryption at Subzero Temperatures

Xiaojie Sui [#], Xiaodong Wang [#], Chengcheng Cai, Junyi Ma, Jing Yang, Lei Zhang [*]

Department of Biochemical Engineering, School of Chemical Engineering and Technology, Frontier Science Center for Synthetic Biology and Key Laboratory of Systems Bioengineering (MOE), Tianjin University, Tianjin 300350, China

ARTICLE INFO

Article history:
Received 9 October 2021
Revised 20 March 2022
Accepted 31 March 2022
Available online 1 February 2023

Keywords:
Freeze-tolerant hydrogels
Aggregation-induced emission
Encryption
Decryption
Anticounterfeiting

ABSTRACT

Freeze-tolerant hydrogels can regulate the freezing behavior of the water inside them at subzero temperatures, thus maintaining their exceptional properties (e.g., intelligent responsiveness and liquid transporting) and extending their applications under cold conditions. Herein, a series of aggregation-induced emission (AIE)-active freeze-tolerant hydrogels are developed, which enable information encryption and decryption at subzero temperatures. The hydrogels possess varied freezing temperatures (T_f) depending on their betaine concentration. Above/below T_f, the information in the hydrogels that is encoded by means of AIE luminogens presents turn-off/-on fluorescence, thereby enabling the use of these hydrogels for information encryption and decryption. Moreover, by tuning the cooling procedures or introducing photothermal copper sulfide nanoparticles into the hydrogels via an *in situ* sulfidation process, together with certain irradiation conditions, multistage information readouts can be obtained, significantly enhancing the information security. Finally, because the decrypted information in the hydrogels is irreversibly sensitive to temperature fluctuation, external energy-free cryogenic anticounterfeiting labels built with the hydrogels are demonstrated, which can realize the visual and real-time viability monitoring of cryopreserved biosamples (e.g., mesenchymal stem cells and red blood cells) during cold-chain transportation (−80 °C).

1. Introduction

Many living organisms in nature (e.g., the chameleon and octopus) have evolved unique properties to change their skin colors for acclimatization, camouflage, and self-protection [1–3]. Researchers have long attempted to mimic these fascinating natural behaviors via soft artificial materials for applications such as confidential information protection and the anticounterfeiting of commercial products [4–14]. In particular, smart hydrogels have received a great deal of attention due to their tissue-like mechanical properties and capability of emitting different colors under external stimuli (e.g., chemicals, pH, or temperature) [4–6,15–25]. For example, Qin et al. [4] reported a hydrogel interferometer with adaptive color change for controllable information encryption. Ji et al. [16] developed several aggregation-induced emission luminogens (AIEgens)-based hydrogels with different colors and used them as building blocks to form a "Rubik's cube" for information storage. Le et al. [6,26,27] and Qiu et al. [28] prepared a series of smart fluorescent hydrogels/organohydrogels to achieve transient information storage, dynamic anticounterfeiting, and on-demand information decryption and transmission, among other applications. These elaborate designs offer new solutions for developing advanced information-protection materials. It is worth noting that, apart from improving the information storage capacity, information security, and durability of these materials, researchers have recently shown great interest in their performance at low temperatures (e.g., in polar regions, aerospace, and cryogenic transport). For example, many high-value products, such as vaccines, antibodies, and therapeutic living cells, are temperature sensitive and greatly rely on cold-chain logistics [29–31]. Anticounterfeiting and the real-time quality monitoring of these products during transportation using smart hydrogels is of great economic significance.

* Corresponding author.
E-mail address: lei_zhang@tju.edu.cn (L. Zhang).
[#] These authors contributed equally to this work.

https://doi.org/10.1016/j.eng.2022.03.021

However, developing soft smart materials for low-temperature applications remains a challenge due to unavoidable damage to materials, such as ice formation induced fractures and inhibited thermodynamic and kinetic processes (e.g., ion transporting, molecular mobility, or chemical reactions) [32,33]. Consequently, their functionalities, such as liquid transporting and intelligent responsiveness to external stimuli, might experience degradation and even failure. Recently, the development of freeze-tolerant hydrogels has opened up opportunities to tackle these problems. By doping antifreezing molecules (e.g., betaine, glycerol, and ethylene glycol) into hydrogels or modifying the polymeric network of hydrogels, it is possible to obtain hydrogels that can endure subzero temperatures and maintain their unique features as soft smart materials [32–41]. For example, Sui et al. [38] introduced betaine or proline into Ca-alginate/polyacrylamide (PAAm) hydrogels, enabling them to remain unfrozen at −40 °C. Zhang et al. [39] fabricated intrinsic freeze-tolerant hydrogels without adding any antifreezing molecules based on the hydrophilic EGINA crosslinker and a tightly crosslinked double-network structure. To date, freeze-tolerant hydrogels have enabled wearable sensors [38,42], actuators [43], and energy storage devices [44,45], among other applications, to operate under cold conditions. However, to the best of our knowledge, the development and use of such smart materials for information protection and anticounterfeiting at subzero temperatures have not been reported.

In this work, we report a series of aggregation-induced emission (AIE)-active freeze-tolerant hydrogels that can intelligently enable information encryption and decryption in subzero environments. AIEgens are organic molecules with strong emissions in aggregated states or solid states due to restricted intramolecular motions [46–48]. Because of the rapid development of water-soluble AIEgens, their applications have been extended to various aqueous environments [18,49]. As is well known, these water-soluble molecules are repelled from the water phase as ice grows, resulting in their accumulation at the water/ice interface [50,51]. Therefore, we assume that the aggregation and fluorescence emission of AIEgens can be manipulated by the freezing behavior of water inside hydrogels, allowing these materials to be applied for controlled information encryption and decryption. The design principle is depicted in Fig. 1. A series of freeze-tolerant hydrogels are fabricated with varied freezing temperatures (T_f) by tuning their betaine concentration. Above T_f, the AIEgens are well dispersed in the hydrogels and exhibit no emissions. Therefore, the information in the hydrogels that is encoded via the AIEgens is encrypted and cannot be read by means of common strategies. Below T_f, the freezing of water inside the hydrogels causes the accumulation of AIEgens at the water/ice interface. As a result, highly luminescent patterns can be recognized for information decryption.

2. Materials and methods

2.1. Materials

Acrylamide (AAm) and *N*,*N*′-methylenebisacrylamide (MBAA) were purchased from Alfa Aesar (China). Ammonium persulfate (APS) and glycerol were obtained from Acors Organics (USA). Betaine and polyvinylpyrrolidone (PVP, M_w = 40 000) were purchased from Sigma Aldrich (China). 2,2′,2″,2‴-((ethane-1,1,2,2-tetrakis(benzene-4,1-diyl)) tetrakis-(oxy)) tetraacetate (TPE-4CO_2Na) was synthesized by Xi'an Qiyue Biotechnology Co., Ltd. (China). Copper(II) acetate monohydrate was purchased from Heowns Biochem Technologies, LLC (China). Sodium hydrosulfide (NaHS) was obtained from Infinity Scientific (China). Milli-Q water (18.2 MΩ·cm) was used in all experiments.

2.2. Preparation of freeze-tolerant Bx-gels

The PAAm hydrogels were prepared as follows. AAm (860 mg), MBAA (0.37 mg), and APS (0.86 mg) were dissolved in pure water (3.44 mL). After removing bubbles, the mixture was injected into home-made polytetrafluoroethylene molds and polymerized at 55 °C for 12 h. Afterward, the PAAm hydrogels were soaked into Bx-solutions (where *x* represents the betaine concentration) until an equilibrated state was achieved.

2.3. Loading procedure of AIEgens in Bx-gels via transfer printing

Filter papers were tailored into the desired shapes and immersed in TPE-4CO_2Na solutions (2 mmol·L^{-1}) for 5 min. Subsequently, the AIEgens-containing papers were used as stamps and attached onto the surface of the B*x*-gels for 10 s. Because of the concentration gradient between the AIEgens stamps and the B*x*-gels, the AIEgens could diffuse into the B*x*-gels, and specific patterns could be printed on the B*x*-gels.

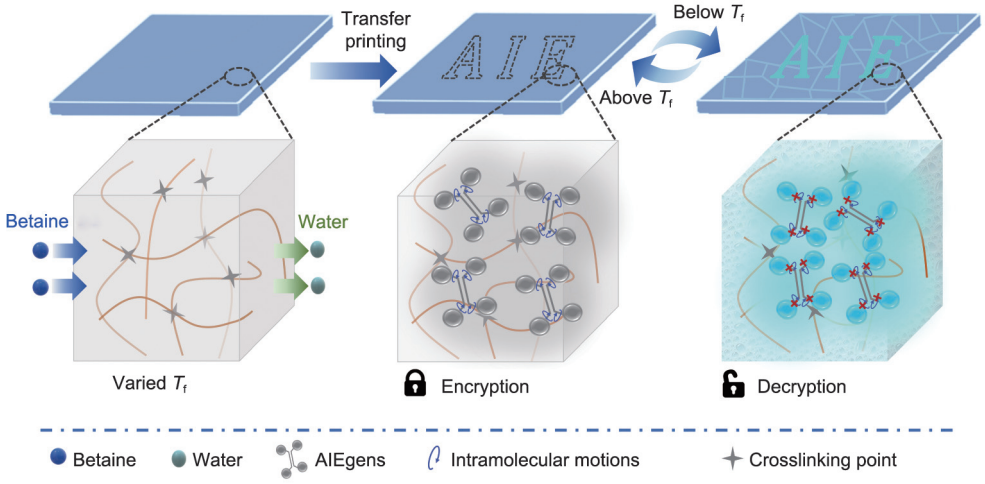

Fig. 1. Schematic drawing of the design principle for information encryption and decryption.

2.4. Differential scanning calorimetry measurement

Samples (5–10 mg) were put in aluminum pans and transferred to a differential scanning calorimetry (DSC) system (DSC 3500 Sirius, NETZSCH, Germany). After equilibration at 25 °C for 5 min, the samples were cooled to −40 °C at a rate of −5 °C·min^{-1} and held at −40 °C for 90 min. Subsequently, the samples were warmed back to 25 °C at a rate of 1 °C·min^{-1} [37]. The onset point of the heat flow curves during the warming process was determined as the T_f of the samples.

2.5. Fluorescence spectra measurement

The fluorescence spectra of samples were measured using a microplate reader (Infinity M200 PRO, Tecan, Switzerland) at an excitation wavelength of 365 nm.

2.6. Synthesis of Cu_2O nanoparticles

Cu_2O nanoparticles (NPs) was synthesized via a modified method reported in the literature [52]. First, under stirring at 1000 r·min^{-1}, PVP (1 g) and copper(II) acetate (0.08 g) were added to ethylene glycol (30 mL), which was followed by a reaction at 70 °C for 30 min. Subsequently, sodium hydroxide (2 mol·L^{-1}, 2 mL) was added to the above mixture and reacted for 30 min. During this process, the solution gradually became dark blue due to the production of copper hydrate. Ascorbic acid solution (0.15 mmol·L^{-1}, 10 mL) was then added to the dark blue solution, which gradually turned dark brown due to the reduction of Cu^{2+}. Finally, Cu_2O NPs was collected and washed three times with water for further use.

2.7. Synthesis of the Cu_2O/Bx-gels

First, AAm (860.00 mg), Cu_2O NPs (11.55 mg), MBAA (2.22 mg), and APS (0.86 mg) were dissolved in pure water (3.44 mL). After removing bubbles, the mixture was injected into the polytetrafluoroethylene molds. After polymerization at 55 °C for 12 h, the hydrogels were immersed in B*x*-solutions to achieve an equilibrated state.

2.8. In situ *sulfidation of Cu_2O NPs*

Filter papers were immersed in NaHS solutions for 5 min. Then, they were attached onto the surface of Cu_2O/B*x*-gels for the *in situ* sulfidation of Cu_2O NPs.

2.9. Cryopreservation of mesenchymal stem cells

Mesenchymal stem cells (MSCs) were purchased from Cryogen Biotechnology Co., Ltd. (China), and cultured in the corresponding medium (OriCell, HUXMA-90011, Cyagen Biosciences Inc., China) under an atmosphere of 5% CO_2. After 90% confluence, the MSCs were detached with 0.25% trypsin–ethylenediaminetetraacetic acid (EDTA) and collected by centrifugation at 1000 r·min^{-1} for 5 min. Subsequently, 1×10^6 MSCs were added to 1 mL of culture medium containing 10% dimethyl sulfoxide (DMSO) (common cryopreservation solutions for MSCs) in cryovials. Afterward, the samples were cooled to −80 °C with a cooling rate of −1 °C·min^{-1} and finally cryopreserved at −80 °C.

2.10. Cryopreservation of rabbit red blood cells

Rabbit red blood cells (RBCs) were purchased from Nanjin Senbeijia Biotechnology Co., Ltd. (China), and stored at 4 °C. Before the experiments, the RBCs were washed twice using phosphate-buffered saline (PBS) solution and collected by centrifugation (2000 r·min^{-1}, 10 min). A 40 μL aliquot of RBCs were added to 40% glycerol (golden standard cryopreservation solutions for RBCs) and then cooled to −80 °C with a cooling rate of −1 °C·min^{-1}.

2.11. Measurement of cell viability of MSCs

The MSCs were stained using a Live/Dead viability kit (Molecular Probes, UK) according to the manufacturer's instructions. After being stained away from light for 30 min, the samples were observed using an inverted microscope (Eclipse Ti-S, Nikon, Japan). The viability was calculated by counting the number of live cells (green) and dead cells (red) [53].

2.12. Measurement of cell viability of RBCs

The supernatant of the samples was added to a 96-well microplate, and the absorbance was measured at 450 nm with a microplate reader (Tecan Infinity M200 PRO). The viability of the RBCs was calculated as follows [53,54]:

$$\text{Cell viability} = 100\% - (A - A_1)/(A_0 - A_1) \times 100\% \quad (1)$$

where A, A_0, and A_1 are the absorbance of the detected samples, negative control samples, and positive control samples, respectively. The negative or positive control samples were equal amounts of fresh RBCs added to PBS solutions or pure water.

3. Results and discussion

3.1. Fluorescence emission of AIEgens modulated by T_f

In nature, various freeze-tolerant plants can accumulate zwitterionic betaine to resist water freezing and enable their survival under cold conditions [55–57]. Herein, we employed betaine as an antifreeze agent to tune the T_f of its aqueous solutions or hydrogels; these are designated as B*x*-solutions or B*x*-gels, where *x* represents the betaine concentration. According to DSC analysis, as the betaine concentration increased, both the B*x*-solutions and the B*x*-gels showed a decreased T_f (Fig. 2(a); Figs. S1(a) and (b) in Appendix A), which was consistent with their freezing behavior observed at subzero temperatures (Figs. S1(c) and (d) in Appendix A). This trend occurred because the betaine strongly interacted with the water molecules via electronically induced hydration effects, consequently impeding the hydrogen-bond network formation of water molecules and inhibiting ice formation [58,59]. Compared with the B*x*-solutions, the B*x*-gels showed a slightly lower T_f because their hydrophilic polymer networks could also bind water molecules via hydrogen-bonding effects and further interfere with ice formation [60].

Next, the fluorescence emissions of a water-soluble AIEgen TPE-4CO_2Na (Fig. S2 in Appendix A) in B*x*-solutions or B*x*-gels with varied T_f were studied. As shown in Fig. S3 in Appendix A, above T_f, the AIEgens exhibited negligible fluorescence in both the B*x*-solutions and B*x*-gels. In stark contrast, they were highly emissive below T_f. This occurred because, as ice grew in the B*x*-solutions or B*x*-gels below T_f, the AIEgens were gradually repelled from the water phase and accumulated at the ice/water interface, resulting in the restriction of intramolecular motions and fluorescence emissions [50,51]. To further verify this mechanism, we investigated the correlation between the water phase states in B*x*-solutions or B*x*-gels and the fluorescence of the AIEgens. As shown in Figs. 2(b) and (c), three regions could be observed in the phase diagrams of the B*x*-solutions or B*x*-gels: the unfrozen water (white region, above T_f), ice–water mixture (grey region, below T_f), and ice (blue region,

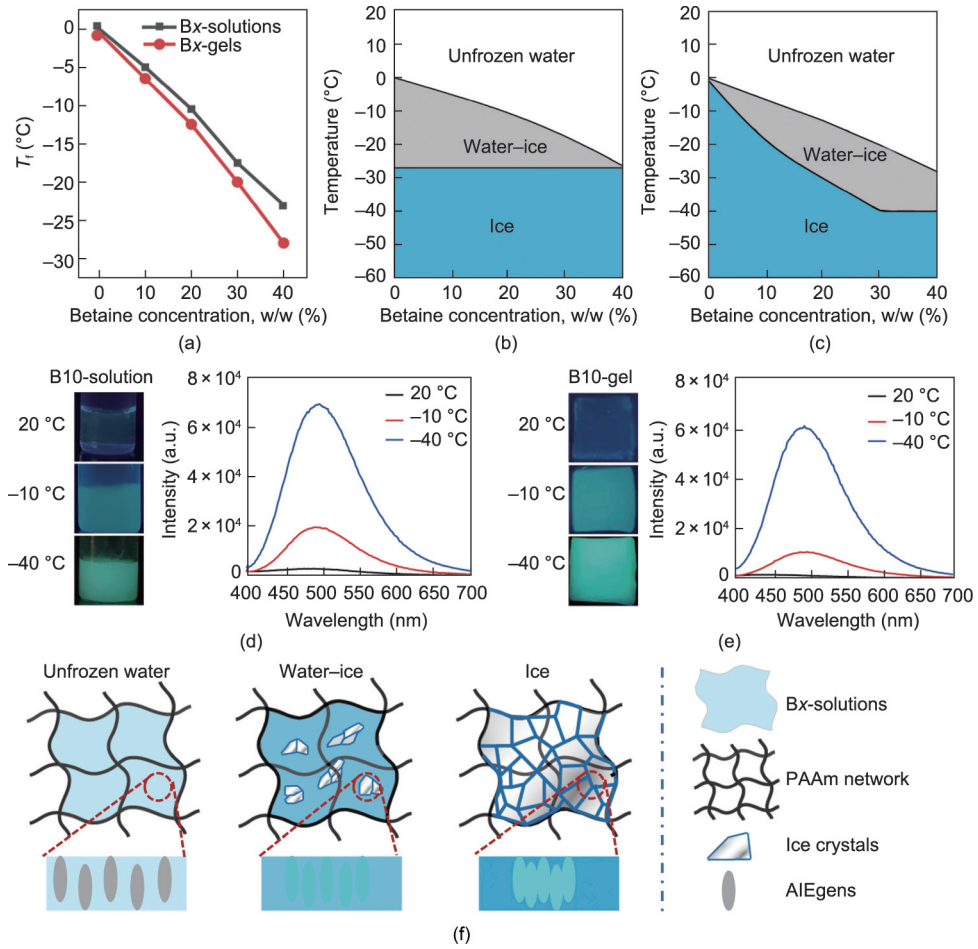

Fig. 2. Fluorescence emissions of the AIEgens modulated by T_f. (a) The T_f of the B*x*-solutions or B*x*-gels. (b, c) Phase diagrams of (b) B*x*-solutions or (c) B*x*-gels, where the white, grey, and blue regions respectively indicate unfrozen water, water–ice mixture, and ice. (d, e) Fluorescence images and fluorescence spectra (λ_{ex} = 365 nm) of (d) B10-solutions and (e) B10-gels at 20 °C (in the white region), −10 °C (in the grey region), and −40 °C (in the blue region), respectively. (f) Schematic drawing of the different aggregation states of AIEgens in B*x*-gels with unfrozen water, water–ice mixture, or ice inside the PAAm hydrogel networks.

below T_f) within the B*x*-solutions or B*x*-gels. Notably, the AIEgens exhibited no emission in the white regions. In comparison, strong fluorescence of the AIEgens was observed in the grey or blue regions. Moreover, at the same betaine concentration, the AIEgens showed higher fluorescence intensity in the blue regions than the grey regions (Figs. 2(d) and (e)), because the increased ice formation induced stronger aggregation of the AIEgens at the water/ice interface (Fig. 2(f)). These results further confirmed that the fluorescence emission of the AIEgens was sensitive to ice formation and could be modulated by T_f.

3.2. Information encryption and decryption using AIE-active B*x*-gels

Due to the tunable fluorescence emissions of the AIEgens in B*x*-gels above/below T_f, we employed the AIEgens as the "ink" and B*x*-gels with different T_f as the "flexible paper" for information encryption and decryption. As a proof of concept (Figs. 3(a) and (b)), a star pattern was respectively printed on the B10-gel (T_f was −6.5 °C) or B40-gel (T_f was −28.0 °C) by means of paper stamps containing AIEgens. Above T_f, due to no ice formation occurring inside the B10-gel or B40-gel, the input AIEgens exhibited no aggregation or fluorescence emission; thus, they could be used to achieve information encryption. At −20 °C with ultraviolet (UV) exposure, the star pattern was only decrypted on the B10-gel, because its freezing caused the emission of the input AIEgens. When the temperature was further decreased to −30 °C, the star pattern showed up on both the B10-gel and the B40-gel. These results demonstrated that the information patterns input via AIEgens could be encrypted in the B*x*-gels above T_f, and that the correct cooling temperature was the key to information decryption.

Interestingly, the decrypted information could be easily erased at temperatures above T_f to prevent secondary information leakage. As shown in Fig. 3(b), the decrypted star patterns all disappeared at 20 °C, and the erasure time decreased as the environmental temperature increased (Fig. 3(c)). This occurred because, as the ice melted at temperatures above T_f, the accumulated AIEgens redissolved in the water phase of the hydrogels and reconstructed their intramolecular rotations, causing the fluorescence to disappear. The redissolved AIEgens were unable to reassemble after a second freezing. Therefore, different patterns could be reprinted on the erased B*x*-gels for repeated encryption and decryption (Fig. S4 in Appendix A), demonstrating the capability of the B*x*-gels for reusage. In addition, by tailoring the shape of the AIEgens-containing paper stamps, diverse information patterns could be input into the hydrogels (Fig. 3(d)).

3.3. Multistage information encryption and decryption with enhanced security

Based on the aforementioned information encryption and decryption principle, we next investigated two approaches to

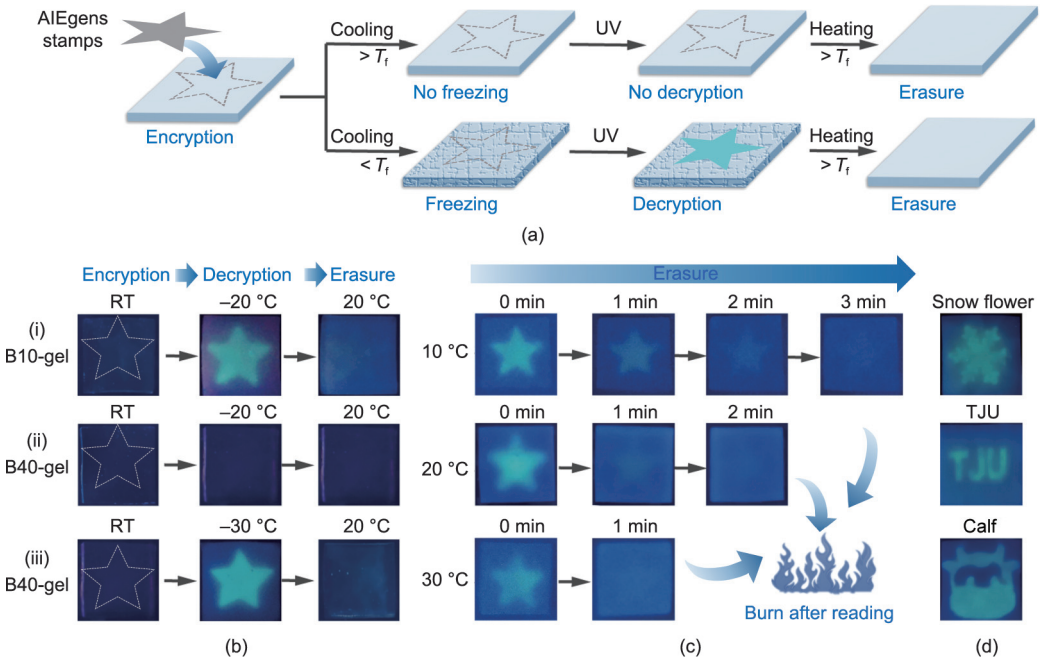

Fig. 3. Information encryption and decryption using AIE-active B*x*-gels. (a) Schematic drawing of the encryption and decryption process. (b) Fluorescence images of the B10-gel or B40-gel input with a star pattern by means of AIEgens at (left) room temperature (RT), (medium) subzero temperatures, or (right) 20 °C. (c) Erasure process of the decrypted B10-gel at temperatures above T_f. (d) Different decrypted information patterns on the B10-gel at −20 °C. All images were taken under a 365 nm UV lamp.

further enhance the information security. One method involved tuning the cooling procedures to achieve multistage information readouts. As shown in Fig. 4(a), the AIE-active B*x*-gels with varied T_f could be used as building blocks to construct and display different numbers at specific subzero temperatures. For a specific construct, with varying cooling procedures, a total of six different readouts could be obtained, as demonstrated in Fig. 4(b). Unless possessing additional knowledge, readers would be unable to recognize which readout was the true message; thus, the information security is enhanced.

Another method involved introducing Cu_2O NPs into the B*x*-gels (Cu_2O/B*x*-gels) as a much safer "flexible paper." As shown in Figs. 4(c) and (d), a star pattern was first encrypted on the Cu_2O/B*x*-gel by means of the paper stamps containing AIEgens. Afterward, partial Cu_2O NPs in hydrogels were converted into photothermal Cu_9S_8 NPs by means of round paper stamps containing NaHS solutions via an *in situ* sulfidation process (Figs. S5(a)–(c) in Appendix A). After cooling to temperatures below T_f, a star pattern first emerged under UV exposure, because ice formation inside the hydrogels resulted in the aggregation and fluorescence emission of the AIEgens. With further near-infrared (NIR) irradiation, a "hollow star" pattern could gradually be seen (Fig. 4(d)). This occurred because the Cu_9S_8 NPs-embedded area had a higher melting rate than the Cu_2O NPs-embedded area in the hydrogels (Fig. S5(d) in Appendix A), resulting in faster fluorescence disappearance. Similarly, as shown in Fig. 4(e), a round pattern was first observed at temperatures below T_f. After further NIR exposure, a smiling face could be seen. These results demonstrated that the correct information pattern could only be recognized when both the cooling conditions and the irradiation conditions were correct.

3.4. Demonstration of cryogenic anticounterfeiting labels for cell viability monitoring

Over the last few decades, cell-based therapy (e.g., stem cells, T cells, and natural killer cells) has emerged as a rising star in the treatment of various refractory human diseases [61–66]. For example, the transplantation of MSCs has been successfully applied to a variety of malignancies and bone marrow failure syndromes [64,67]. Before transplantation, these therapeutic living cells require cryopreservation (< −80 °C) and cryogenic transportation for allocation over long distances [30,68]. However, during cryogenic transportation, these cryopreserved cells are sensitive to temperature fluctuation [69,70]. During fluctuation, detrimental ice recrystallization can occur in the samples [31,71]. Consequently, these therapeutic cells can be damaged, resulting in severe cell waste and affecting their clinical applications. Therefore, monitoring the temperature rise is of great significance during cryogenic transportation. Currently, live/dead staining assays are the most commonly used method to detect cell viability [31]. However, such an assay requires sophisticated equipment (e.g., a fluorescence microscope), and the detection process is complicated; thus, these assays cannot achieve real-time cell viability monitoring during cryogenic transportation.

As shown in Fig. S6 in Appendix A, a series of AIE-active B*x*-gels were fabricated and encrypted with a checkmark sign which was visible under UV irradiation at a cryogenic temperature (−80 °C). After experiencing a temperature rise to 20 °C for different periods and then put back to −80 °C, the decrypted checkmarks on the hydrogels became fuzzy or even disappeared under UV irradiation. Moreover, the clarity of the decrypted patterns was negatively related to the exposure time at 20 °C and was positively related to the betaine concentrations of the hydrogels. Due to this finding, we next employed AIE-active B*x*-gels as cryogenic anticounterfeiting labels attached to the outside of cryogenic vials in order to indicate the temperature rise and further monitor the cell viability during cryogenic transportation (Fig. 5(a)). Herein, MSCs and rabbit RBCs were used as model cells to demonstrate this concept. As shown in Figs. 5(b) and (c), after experiencing a temperature rise to 20 °C, the viability of the MSCs decreased significantly, and longer exposure time at 20 °C led to lower viability. Notably, this downward trend in cell viability could be matched with the clarity of the decrypted checkmarks

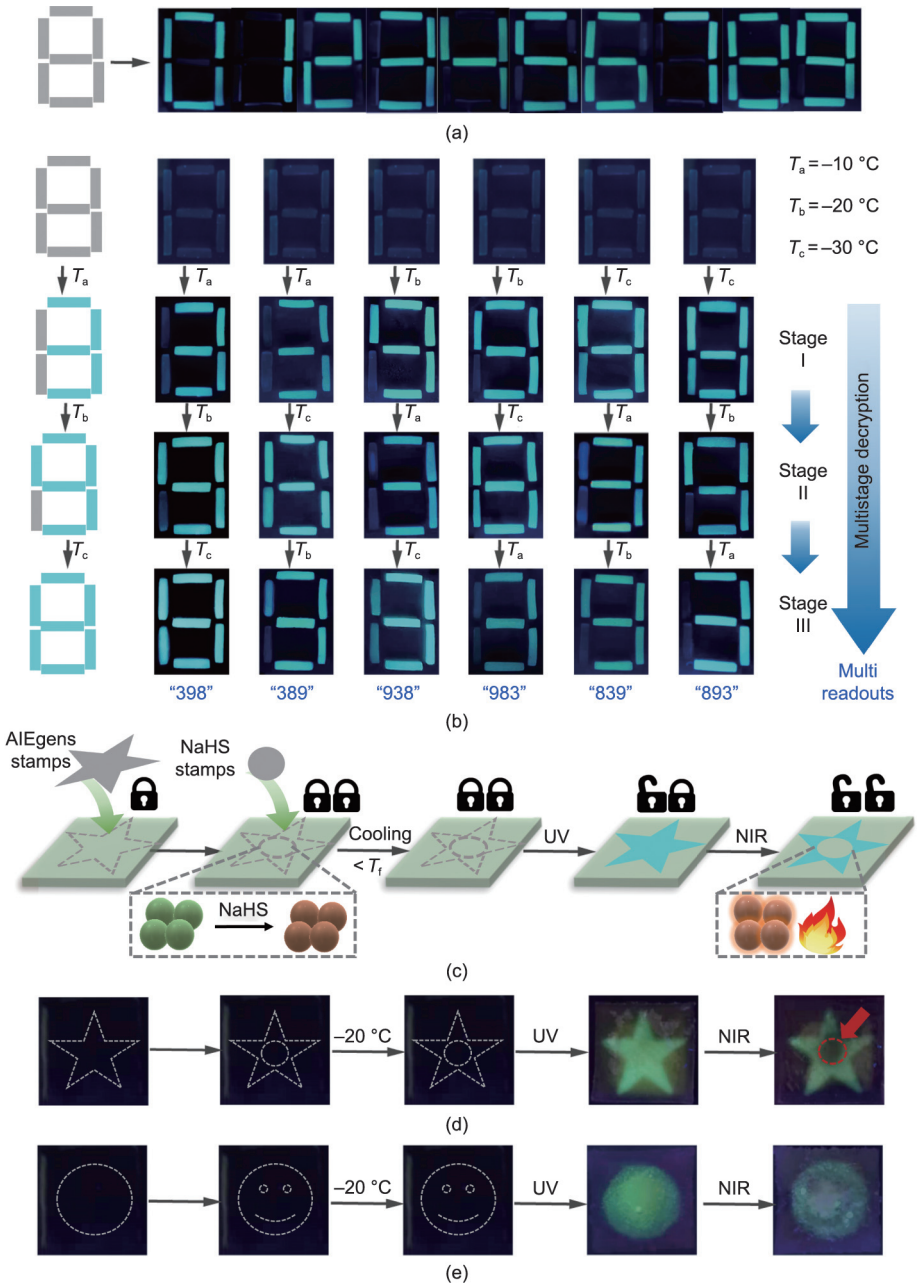

Fig. 4. Multistage information encryption and decryption. (a) Images of numbers displayed by the assembled AIE-active B*x*-gels. (b) Different multistage readouts of the numbers obtained by altering the cooling procedures. (c) Schematic drawing of photothermal NPs being introduced into AIE-active B*x*-gels for multistage information encryption and decryption and (d, e) two examples as a proof of this concept. All photos were taken under a 365 nm UV lamp. NIR: near-infrared.

on AIE-active B20-gels (Fig. 5(d)). Similar results were found for the RBCs (Fig. S7 in Appendix A). These results demonstrated that the cryogenic anticounterfeiting labels built with the AIE-active B*x*-gels can be used to provide real-time cell viability information to manufacturers or consumers in a visual way, without requiring external energy.

4. Conclusions

In summary, we have developed a series of AIE-active freeze-tolerant hydrogels. The uniqueness of these smart materials lies in their capability for information encryption and decryption under subzero temperatures. This information-protection strategy relies on zwitterionic betaine-based freeze-tolerant hydrogels with varied T_f, which provide platforms to regulate the fluorescence off/on performance of AIEgens above/below T_f. Thus, the information that is input into the hydrogels via AIEgens can be encrypted and decrypted. Notably, by tuning the cooling procedures or introducing photothermal NPs into the hydrogels, together with certain irradiation conditions, different multistage information can be obtained. This significantly enhances the information security, because these specially predesigned decryption procedures are only accessible to the authorized party. We also demonstrated cryogenic anticounterfeiting labels built with the hydrogels for the visual and real-time monitoring of cell viability during cryogenic transportation; the labels are energy-free and are expected to be important to the allocation of biosamples in cell-based therapy.

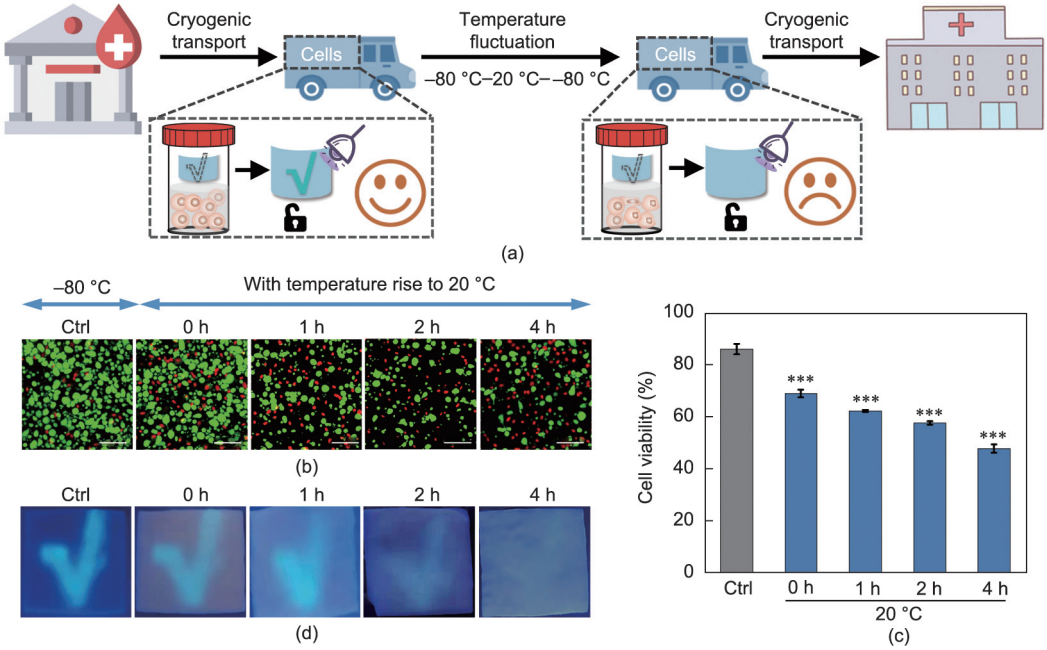

Fig. 5. Demonstration of cryogenic anticounterfeiting labels using AIE-active B*x*-gels for cell viability monitoring. (a) Schematic drawing of how the AIE-active B*x*-gels respond to temperature fluctuations and monitor cell viability during cryogenic transport. (b) Fluorescence images of the live/dead staining assay of MSCs. (c) Cell viability of MSCs ($n = 3$). (d) Fluorescence images of decrypted AIE-active B20-gels without experiencing temperature change (Ctrl), or experiencing a temperature rise to 20 °C from −80 °C for 0, 1, 2, or 4 h. Green: live cells; red: dead cells. ***$P < 0.005$. Scale bar = 100 μm.

Acknowledgments

The authors acknowledge financial support from the National Natural Science Foundation of China (22078238, 21961132005, and 21908160) and the National Key Research and Development Program of China (2022YFC2104800 and 2021YFC2100800).

Compliance with ethics guidelines

Xiaojie Sui, Xiaodong Wang, Chengcheng Cai, Junyi Ma, Jing Yang, and Lei Zhang declare that they have no conflict of interest or financial conflicts to disclose.

Appendix A. Supplementary data

Supplementary material to this article can be found online at https://doi.org/10.1016/j.eng.2022.03.021.

References

[1] Teyssier J, Saenko SV, van der Marel D, Milinkovitch MC. Photonic crystals cause active colour change in chameleons. Nat Commun 2015;6(1):6368.
[2] Mäthger LM, Hanlon RT. Malleable skin coloration in cephalopods: selective reflectance, transmission and absorbance of light by chromatophores and iridophores. Cell Tissue Res 2007;329(1):179–86.
[3] Mäthger LM, Denton EJ, Marshall NJ, Hanlon RT. Mechanisms and behavioural functions of structural coloration in cephalopods. J R Soc Interface 2009;6 (Suppl 2):S149–63.
[4] Qin M, Sun M, Bai R, Mao Y, Qian X, Sikka D, et al. Bioinspired hydrogel interferometer for adaptive coloration and chemical sensing. Adv Mater 2018;30(21):1800468.
[5] Ji X, Wu RT, Long L, Ke XS, Guo C, Ghang YJ, et al. Encoding, reading, and transforming information using multifluorescent supramolecular polymeric hydrogels. Adv Mater 2018;30(11):1705480.
[6] Le X, Shang H, Yan H, Zhang J, Lu W, Liu M, et al. A urease-containing fluorescent hydrogel for transient information storage. Angew Chem Int Ed Engl 2021;60(7):3640–6.
[7] Ding L, Wang XD. Luminescent oxygen-sensitive ink to produce highly secured anticounterfeiting labels by inkjet printing. J Am Chem Soc 2020;142 (31):13558–64.
[8] Qin L, Liu X, He K, Yu G, Yuan H, Xu M, et al. Geminate labels programmed by two-tone microdroplets combining structural and fluorescent color. Nat Commun 2021;12(1):699.
[9] Li Z, Chen H, Li B, Xie Y, Gong X, Liu X, et al. Photoresponsive luminescent polymeric hydrogels for reversible information encryption and decryption. Adv Sci 2019;6(21):1901529.
[10] Zhang Y, Le X, Jian Y, Lu W, Zhang J, Chen T. 3D fluorescent hydrogel origami for multistage data security protection. Adv Funct Mater 2019;29 (46):1905514.
[11] Wang H, Ji X, Page ZA, Sessler JL. Fluorescent materials-based information storage. Mater Chem Front 2020;4(4):1024–39.
[12] Hou Y, Li Z, Hou J, Shi P, Li Y, Niu M, et al. Conditional mechanochromic fluorescence with turn-on response: a new way to encrypt and decrypt binary data. Dyes Pigm 2018;159:252–61.
[13] Zhang M, Li Y, Gao K, Li Z, Liu Y, Liao Y, et al. A turn-on mechanochromic luminescent material serving as pressure sensor and rewritable optical data storage. Dyes Pigm 2020;173:107928.
[14] Lu L, Wang K, Wu H, Qin A, Tang BZ. Simultaneously achieving high capacity storage and multilevel anti-counterfeiting using electrochromic and electrofluorochromic dual-functional AIE polymers. Chem Sci 2021;12 (20):7058–65.
[15] Wei S, Li Z, Lu W, Liu H, Zhang J, Chen T, et al. Multicolor fluorescent polymeric hydrogels. Angew Chem Int Ed Engl 2021;60(16):8608–24.
[16] Ji X, Li Z, Liu X, Peng HQ, Song F, Qi J, et al. A functioning macroscopic "Rubik's cube" assembled via controllable dynamic covalent interactions. Adv Mater 2019;31(40):1902365.
[17] Sun J, Wang J, Chen M, Pu X, Wang G, Li L, et al. Fluorescence turn-on visualization of microscopic processes for self-healing gels by AIEgens and anticounterfeiting application. Chem Mater 2019;31(15):5683–90.
[18] Li Z, Ji X, Xie H, Tang BZ. Aggregation-induced emission-active gels: fabrications, functions, and applications. Adv Mater 2021;33(33):2100021.
[19] Bat E, Lin EW, Saxer S, Maynard HD. Morphing hydrogel patterns by thermo-reversible fluorescence switching. Macromol Rapid Commun 2014;35 (14):1260–5.
[20] Yuk H, Lu B, Zhao X. Hydrogel bioelectronics. Chem Soc Rev 2019;48 (6):1642–67.
[21] Won P, Kim KK, Kim H, Park JJ, Ha I, Shin J, et al. Transparent soft actuators/sensors and camouflage skins for imperceptible soft robotics. Adv Mater 2021;33(19):2002397.
[22] Wu S, Shi H, Lu W, Wei S, Shang H, Liu H, et al. Aggregation-induced emissive carbon dots gels for octopus-inspired shape/color synergistically adjustable actuator. Angew Chem Int Ed Engl 2021;60(40):21890–8.
[23] Larson C, Peele B, Li S, Robinson S, Totaro M, Beccai L, et al. Highly stretchable electroluminescent skin for optical signaling and tactile sensing. Science 2016;351(6277):1071–4.
[24] Ilami M, Bagheri H, Ahmed R, Skowronek EO, Marvi H. Materials, actuators, and sensors for soft bioinspired robots. Adv Mater 2021;33(19):2003139.

[25] Zhu CN, Bai T, Wang H, Ling J, Huang F, Hong W, et al. Dual-encryption in a shape-memory hydrogel with tunable fluorescence and reconfigurable architecture. Adv Mater 2021;33(29):2102023.
[26] Le X, Shang H, Wu S, Zhang J, Liu M, Zheng Y, et al. Heterogeneous fluorescent organohydrogel enables dynamic anti-counterfeiting. Adv Funct Mater 2021;31(52):2108365.
[27] Le X, Shang H, Gu S, Yin G, Shan F, Li D, et al. Fluorescent organohydrogel with thermal-induced color change for anti-counterfeiting. Chin J Chem 2022;40 (3):337–42.
[28] Qiu H, Wei S, Liu H, Zhan B, Yan H, Lu W, et al. Programming multistate aggregation-induced emissive polymeric hydrogel into 3D structures for on-demand information decryption and transmission. Adv Intell Syst 2021;3 (6):2000239.
[29] Choi S, Eom Y, Kim SM, Jeong DW, Han J, Koo JM, et al. A self-healing nanofiber-based self-responsive time-temperature indicator for securing a cold-supply chain. Adv Mater 2020;32(11):1907064.
[30] Giwa S, Lewis JK, Alvarez L, Langer R, Roth AE, Church GM, et al. The promise of organ and tissue preservation to transform medicine. Nat Biotechnol 2017;35 (6):530–42.
[31] Chang T, Zhao G. Ice inhibition for cryopreservation: materials, strategies, and challenges. Adv Sci 2021;8(6):2002425.
[32] Rong Q, Lei W, Huang J, Liu M. Low temperature tolerant organohydrogel electrolytes for flexible solid-state supercapacitors. Adv Energy Mater 2018;8 (31):1801967.
[33] Zhang XF, Ma X, Hou T, Guo K, Yin J, Wang Z, et al. Inorganic salts induce thermally reversible and anti-freezing cellulose hydrogels. Angew Chem Int Ed Engl 2019;58(22):7366–70.
[34] Jian Y, Handschuh-Wang S, Zhang J, Lu W, Zhou X, Chen T. Biomimetic anti-freezing polymeric hydrogels: keeping soft-wet materials active in cold environments. Mater Horiz 2021;8(2):351–69. Correction in: Mater Horiz 2020;7(12):3339.
[35] Zhou D, Chen F, Handschuh-Wang S, Gan T, Zhou X, Zhou X. Biomimetic extreme-temperature- and environment-adaptable hydrogels. ChemPhysChem 2019;20(17):2139–54.
[36] Chen F, Zhou D, Wang J, Li T, Zhou X, Gan T, et al. Rational fabrication of anti-freezing, non-drying tough organohydrogels by one-pot solvent displacement. Angew Chem Int Ed Engl 2018;57(22):6568–71.
[37] Morelle XP, Illeperuma WR, Tian K, Bai R, Suo Z, Vlassak JJ. Highly stretchable and tough hydrogels below water freezing temperature. Adv Mater 2018;30 (35):1801541.
[38] Sui X, Guo H, Chen P, Zhu Y, Wen C, Gao Y, et al. Zwitterionic osmolyte-based hydrogels with antifreezing property, high conductivity, and stable flexibility at subzero temperature. Adv Funct Mater 2020;30(7):1907986.
[39] Zhang D, Liu Y, Liu Y, Peng Y, Tang Y, Xiong L, et al. A general crosslinker strategy to realize intrinsic frozen resistance of hydrogels. Adv Mater 2021;33 (42):2104006.
[40] Rong Q, Lei W, Chen L, Yin Y, Zhou J, Liu M. Anti-freezing, conductive self-healing organohydrogels with stable strain-sensitivity at subzero temperatures. Angew Chem Int Ed Engl 2017;56(45):14159–63.
[41] Han L, Liu K, Wang M, Wang K, Fang L, Chen H, et al. Mussel-inspired adhesive and conductive hydrogel with long-lasting moisture and extreme temperature tolerance. Adv Funct Mater 2018;28(3):1704195.
[42] Zhang W, Wu B, Sun S, Wu P. Skin-like mechanoresponsive self-healing ionic elastomer from supramolecular zwitterionic network. Nat Commun 2021;12 (1):4082.
[43] Jian Y, Wu B, Le X, Liang Y, Zhang Y, Zhang D, et al. Antifreezing and stretchable organohydrogels as soft actuators. Research 2019;2019:2384347.
[44] Jin X, Song L, Yang H, Dai C, Xiao Y, Zhang X, et al. Stretchable supercapacitor at −30 °C. Energy Environ Sci 2021;14(5):3075–85.
[45] Pei Z, Yuan Z, Wang C, Zhao S, Fei J, Wei L, et al. A flexible rechargeable zinc–air battery with excellent low-temperature adaptability. Angew Chem Int Ed Engl 2020;59(12):4793–9.
[46] Hong Y, Lam JWY, Tang BZ. Aggregation-induced emission: phenomenon, mechanism and applications. Chem Commun 2009;29(29):4332–53.
[47] Hong Y, Lam JWY, Tang BZ. Aggregation-induced emission. Chem Soc Rev 2011;40(11):5361–88.
[48] Yang Y, Zhang S, Zhang X, Gao L, Wei Y, Ji Y. Detecting topology freezing transition temperature of vitrimers by AIE luminogens. Nat Commun 2019;10 (1):3165.
[49] Yao H, Wang J, Fan YQ, Zhou Q, Guan XW, Kan XT, et al. Supramolecular hydrogel-based AIEgen: construction and dual-channel recognition of negative charged dyes. Dyes Pigm 2019;167:16–21.
[50] He Z, Liu P, Zhang S, Yan J, Wang M, Cai Z, et al. A freezing-induced turn-on imaging modality for real-time monitoring of cancer cells in cryosurgery. Angew Chem Int Ed Engl 2019;58(12):3834–7.
[51] Miyagawa A, Harada M, Fukuhara G, Okada T. Space size-dependent transformation of tetraphenylethylene carboxylate aggregates by ice confinement. J Phys Chem B 2020;124(11):2209–17.
[52] An L, Wang X, Rui X, Lin J, Yang H, Tian Q, et al. The *in situ* sulfidation of Cu_2O by endogenous H_2S for colon cancer theranostics. Angew Chem Int Ed Engl 2018;57(48):15782–6.
[53] Yang J, Pan C, Zhang J, Sui X, Zhu Y, Wen C, et al. Exploring the potential of biocompatible osmoprotectants as highly efficient cryoprotectants. ACS Appl Mater Interfaces 2017;9(49):42516–24.
[54] Sui X, Wen C, Yang J, Guo H, Zhao W, Li Q, et al. Betaine combined with membrane stabilizers enables solvent-free whole blood cryopreservation and one-step cryoprotectant removal. ACS Biomater Sci Eng 2019;5(2):1083–91.
[55] Nomura M, Muramoto Y, Yasuda S, Takabe T, Kishitani S. The accumulation of glycinebetaine during cold acclimation in early and late cultivars of barley. Euphytica 1995;83(3):247–50.
[56] Kishitani S, Watanabe K, Yasuda S, Arakawa K, Takabe T. Accumulation of glycinebetaine during cold acclimation and freezing tolerance in leaves of winter and spring barley plants. Plant Cell Environ 1994;17(1):89–95.
[57] Yang J, Sui X, Wen C, Pan C, Zhu Y, Zhang J, et al. A hemocompatible cryoprotectant inspired by freezing-tolerant plants. Colloids Surf B Biointerfaces 2019;176:106–14.
[58] Shao Q, Jiang S. Molecular understanding and design of zwitterionic materials. Adv Mater 2015;27(1):15–26.
[59] Kiani H, Sun DW. Water crystallization and its importance to freezing of foods: a review. Trends Food Sci Technol 2011;22(8):407–26.
[60] Song G, Zhang L, He C, Fang DC, Whitten PG, Wang H. Facile fabrication of tough hydrogels physically cross-linked by strong cooperative hydrogen bonding. Macromolecules 2013;46(18):7423–35.
[61] Fang F, Xiao W, Tian Z. Challenges of NK cell-based immunotherapy in the new era. Front Med 2018;12(4):440–50.
[62] Shimasaki N, Jain A, Campana D. NK cells for cancer immunotherapy. Nat Rev Drug Discov 2020;19(3):200–18.
[63] Labanieh L, Majzner RG, Mackall CL. Programming CAR-T cells to kill cancer. Nat Biomed Eng 2018;2(6):377–91.
[64] Tewary M, Shakiba N, Zandstra PW. Stem cell bioengineering: building from stem cell biology. Nat Rev Genet 2018;19(10):595–614.
[65] He W. Cell therapy: pharmacological intervention enters a third era. Engineering 2019;5(1):5–9.
[66] Lu L, Tian Z, Wang X. Cell therapy: a new era of disease intervention. Engineering 2019;5(1):3–4.
[67] Chen J, Hu C, Chen L, Tang L, Zhu Y, Xu X, et al. Clinical study of mesenchymal stem cell treatment for acute respiratory distress syndrome induced by epidemic influenza A (H7N9) infection: a hint for COVID-19 treatment. Engineering 2020;6(10):1153–61.
[68] Scudellari M. Cryopreservation aims to engineer novel ways to freeze, store, and thaw organs. Proc Natl Acad Sci USA 2017;114(50):13060–2.
[69] Pogozhykh D, Pogozhykh O, Prokopyuk V, Kuleshova L, Goltsev A, Blasczyk R, et al. Influence of temperature fluctuations during cryopreservation on vital parameters, differentiation potential, and transgene expression of placental multipotent stromal cells. Stem Cell Res Ther 2017;8(1):66.
[70] Germann A, Oh YJ, Schmidt T, Schön U, Zimmermann H, von Briesen H. Temperature fluctuations during deep temperature cryopreservation reduce PBMC recovery, viability and T-cell function. Cryobiology 2013;67 (2):193–200.
[71] Huebinger J, Han HM, Hofnagel O, Vetter IR, Bastiaens PIH, Grabenbauer M. Direct measurement of water states in cryopreserved cells reveals tolerance toward ice crystallization. Biophys J 2016;110(4):840–9.